International Journal of Minerals, Metallurgy and Materials
Volume 19, Number 12, Dec 2012, Page 1128
DOI: 10.1007/s12613-012-0681-4

Effect of oxygen on the microstructure and mechanical properties of Ti-23Nb-0.7Ta-2Zr alloy

Hui-ping Duan[1)], *Hong-xia Xu*[1)], *Wen-huang Su*[1)], *Yu-bin Ke*[2)], *Zeng-qian Liu*[1)], *and Hong-hai Song*[1)]

1) School of Materials Science and Engineering, Beihang University, Beijing 100191, China
2) Institute of High Energy Physics, Chinese Academy of Science, Beijing 100049, China
(Received: 11 February 2012; revised: 15 April 2012; accepted: 17 April 2012)

Abstract: The influence of oxygen content on the microstructure and mechanical properties of Ti-23Nb-0.7Ta-2Zr (at%) alloy in as-cast and cold-rolled states was investigated systematically in this paper. It is found that the alloy containing oxygen element is only composed of a single β phase, while the alloy without oxygen element consisted of β and α″ phases. Although the grain size becomes larger, the elastic deformation ratio, strength, and hardness of the alloy are all increased with an increase of oxygen content. The as-cast alloy has excellent plastic deformation ability, but the cold-rolled alloy containing oxygen element exhibits brittle characteristics. A conclusion can be drawn that oxygen element can stabilize β phase, inhibit the phase transformation from β to α″, and furthermore help to increase the strength and elastic deformation ability of the alloy.

Keywords: titanium alloys; oxygen; cold rolling; microstructure; mechanical properties

1. Introduction

β-Ti alloys are widely used in aerospace, automotive, and surgical fields because of their attractive properties, such as high strength-to-density ratio, good heat and corrosion resistance, excellent biocompatibility and fatigue performance [1-3]. Among Ti-based alloys, bcc Ti-Nb-Ta-Zr alloys (e.g., Gum Metal) with some content of oxygen exhibit low elastic modulus, high yield strain and high ductility and have attracted considerable attention. Many works have been carried out mainly focusing on their properties and deformation mechanism [4-12]. It was reported that Gum Metal prepared by complicated powder metallurgy (PM) processing showed a unique dislocation-free deformation mechanism, inferring that the Zr-O atom clusters could inhibit the dislocation activity effectively [4].

The content of oxygen element is a decisive factor in determining the microstructure and properties of Gum Metal, and it lies in the range from 0.7at% to 3at% to obtain the superior properties [4]. Kuramoto *et al.* [13] had systematically investigated the effects of oxygen on the properties of Gum Metal and showed that the elastic limit reached 1% and 2.5% with oxygen contents of 0.3at% and 1at% respectively. The dependence of the microstructure and grain size on oxygen content in a melted Ti-Nb-Ta-Zr alloy was also investigated by Wei *et al.* [14]. However, there is a controversy in defining the role of oxygen. Some research results show that oxygen is an α-stabilizer [8, 15], while Qazi *et al.* [16] pointed out that oxygen acted as a β-stabilizer in the solution treatment condition.

To clarify the effect of oxygen on the phase stability, smelt Ti alloys with different oxygen contents in as-cast and cold-rolled states were used in the present work. X-ray diffraction (XRD) and transmission electron microscopy (TEM) were employed to investigate the microstructure and an Instron material testing system was used to test the mechanical properties of the alloys.

2. Experimental

Ti-23Nb-0.7Ta-2Zr-*x*O (at%; *x*=0, 1, and 2; and the corresponding alloy was termed as 0O, 1O, and 2O, respectively) alloys were fabricated with a vacuum non-consuma-

Corresponding author: Wen-huang Su E-mail: suwenhuang6688@126.com
© University of Science and Technology Beijing and Springer-Verlag Berlin Heidelberg 2012

ble arc melting furnace under the protection of argon, using the mixtures of sponge Ti (~96.7wt% in purity), foils of Nb (~99.9wt% purity), pieces of pure Ta (~99.7wt% in purity) and Zr (purity > 99.7wt%). Oxygen was introduced into the alloys in the form of TiO_2 powders, which were pre-compacted to thin discs and then wrapped by a piece of Nb before melting. The ingot (about 120 g) was remelted 8 times to ensure compositional homogeneity. The center part of the ingot was cut into slices with the thickness of 0.5 and 6.1 mm, respectively. The surfaces of the 6.1-mm thick slices were mechanically grinded into a thickness of about 6 mm and then the slices were cold rolled to a reduction of 90% in thickness.

The oxygen content of the alloy was measured by chemical analysis. Phase constitutions were detected on a Bruker D8 XRD using Cu K_α radiation at a rate of 2°/min from 25° to 75°. Specimens for optical observations were mechanically polished and etched using a solution of $HF:HNO_3:H_2O$=1:4:7 (in volume ratio). The slices with the thickness of 0.5 mm were mechanically thinned and polished to thin foils with the thickness of about 30 μm. TEM samples were extracted from the polished thin foils and then thinned by a twin-jet electrolytic polisher in a methanol solution of 6vol% perchloric acid and 34vol% butyl alcohol at temperatures of –30°C to –20°C and voltages of 15-30 V. TEM observations were carried out using a JEM 2100F microscope.

Tensile samples with the gauge dimension of 7.6 mm×3 mm×0.5 mm at the as-cast state and 18 mm×5 mm×0.6 mm at the cold rolling state were machined from the as-cast ingot and the cold-rolled slices, respectively. Tensile tests were carried out on an INSTRON 8801 materials testing machine at a strain of 6.67×10^{-4} s^{-1} for the as-cast samples and 4×10^{-4} s^{-1} for the cold-rolled samples, respectively. Morphology observations of the tensile fracture were performed on a CanScan 3400 scanning electron microscope (SEM). Vickers hardness was also measured by an HXZ-1000 tester.

3. Results and discussion

3.1. Microstructure

Table 1 lists the oxygen content of the alloys. Because of the oxidation of the raw material, there is some oxygen element in the 0O alloy. The actual oxygen content of the alloy is in good agreement with the designed content.

Table 1. Oxygen content of the as-cast Ti-23Nb-0.7Ta-2Zr-*x*O alloys

Alloy	Oxygen content / wt%	Oxygen content / at%
0O	0.05	0.20
1O	0.30	1.15
2O	0.66	2.48

Fig. 1 shows the XRD patterns of the alloys. It can be found that there are characteristic peaks for α″ and β phases in the 0O alloy, but only peaks for β phase in the 1O and 2O alloys, implying that 1O and 2O alloys consist solely of β phase and the 0O alloy is composed of α″ and β phases. It means that the phase transformation from β to α″ phase has been inhibited by the additive of oxygen element, because of the decrease of martensitic transformation temperature from β to α″, which was previously verified by the investigation on Ti-23Nb (at%) and Ti-23Nb-1.0O (at%) alloys [17]. Moreover, except for the change in relative peak density caused by the preferred orientation change, no extra peaks could be found in the XRD patterns of the 1O and 2O alloys after cold rolling.

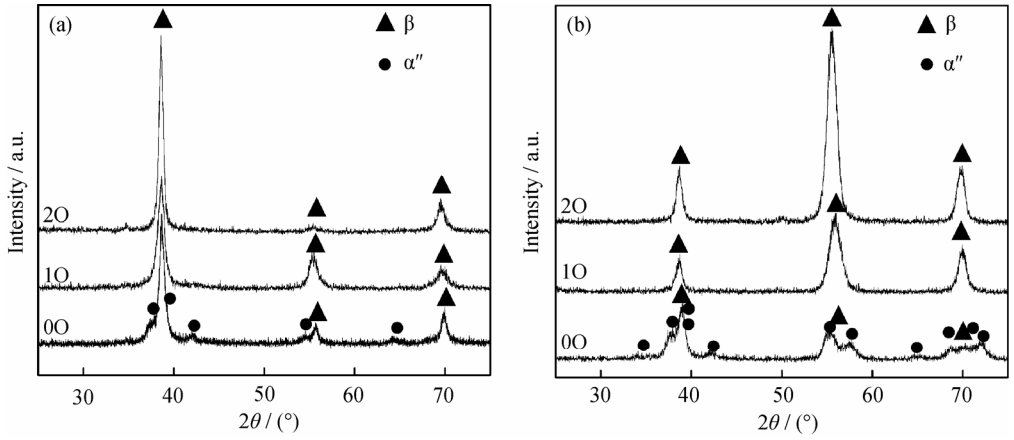

Fig. 1. XRD patterns of Ti-23Nb-0.7Ta-2Zr-*x*O alloys: (a) as-cast; (b) cold-rolled.

It is well known that the phase transformation routine from β to α is different with the composition and external stress state of the Ti alloys. In most cases, β phase cannot transform directly to α phase, but experiences an intermediate process, leading to the occurrence of some intermediate phases, such as α′, α″ or ω phase. In our experiment, XRD analysis confirms that a phase transformation from β to α″ happens in the 0O alloy and the similar phase transformation is not found in the as-cast or cold-rolled 1O and 2O alloys. It demonstrates that oxygen element can stabilize β phase in Ti-23Nb-0.7Ta-2Zr alloy.

If there is a secondary phase in the alloy, it will impede grain growth during cooling and make the grain size smaller. The above XRD analysis confirms that the 0O alloy consists of β and α″ phases and the 1O and 2O alloys is only composed of β phase. Therefore, it is reasonable to deduce that the grains size of the 1O and 2O alloys must be greater than that of the 0O alloy. Fig. 2 shows the optical morphologies of the as-cast 0O, 1O, and 2O alloys. It can be seen that grains in the 1O and 2O alloys are much coarser than those in the 0O alloy. The average grain size of the alloys is about 200, 770, and 930 μm for the 0O, 1O, and 2O alloys, respectively. Therefore, the addition of oxygen element cannot refine the grain size of the alloy but increase the grain size sharply, which implies that second phase exists in the 0O alloy.

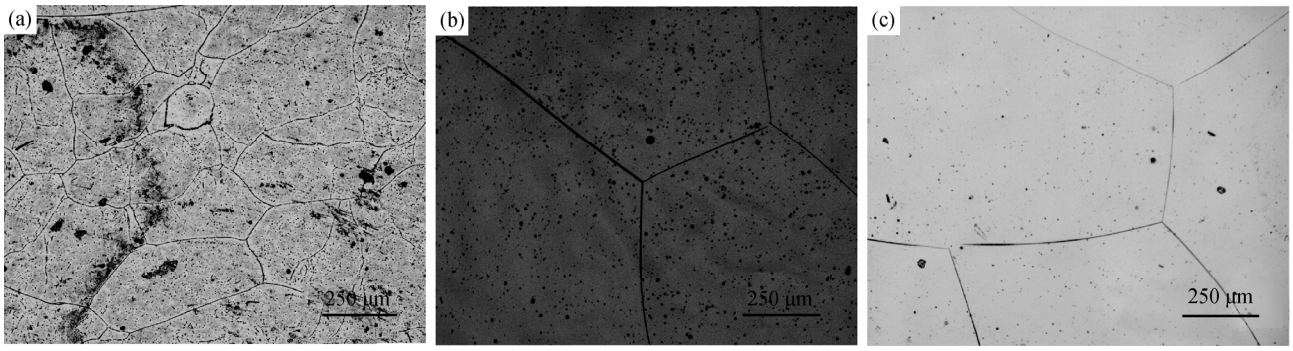

Fig. 2. Optical morphologies of the as-cast Ti-23Nb-0.7Ta-2Zr-*x*O alloys: (a) 0O; (b) 1O; (c) 2O.

3.2. Mechanical properties

The effects of oxygen content and cold rolling on the mechanical properties of the alloys will be evaluated by tensile test, hardness measurement and fracture analysis. Fig. 3 shows the tensile stress-strain curves and Vickers hardness of the alloys. From the stress-strain curves showed in Fig. 3(a), it can be found that the as-cast alloys have good plastic deformation ability and the corresponding stress-strain curves exhibit a stress plateau, indicating that a martensite phase transformation occurs. On the contrary, the cold-rolled alloys exhibit poor plastic deformation ability and no stress plateau appears in the stress-train curves. During test, the cold-rolled 1O and 2O alloys broke immediately after yielding except for the cold-rolled 0O sample.

Table 2 lists the mechanical properties of the alloys measured from the stress-train curves shown in Fig. 3(a), where σ_y, σ_b, σ_f, δ_e, and δ represent the yield strength, tensile strength, fracture strength, elastic deformation ratio, and

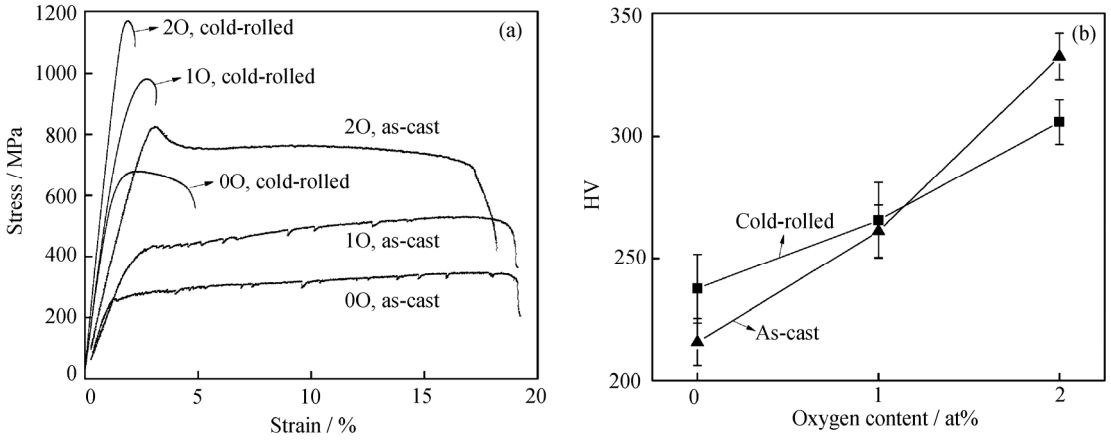

Fig. 3. Mechanical properties of the Ti-23Nb-0.7Ta-2Zr-*x*O (*x*=0, 1, 2) alloys: (a) tensile stress-strain curves; (b) Vickers hardness.

Table 2. Mechanical properties of the alloys measured from the stress-strain curves

Alloys	As-cast					Cold-rolled				
	σ_y/ MPa	σ_b/ MPa	σ_f/ MPa	δ_e/ %	δ/ %	σ_y/ MPa	σ_b/ MPa	σ_f/ MPa	δ_e/ %	δ/ %
0O	230	255	349	1.12	18.76	620	680	615	1.24	4.89
1O	395	421	532	1.44	18.43	910	984	950	1.57	2.83
2O	790	828	684	2.08	17.13	1150	1170	1130	1.76	2.15

total deformation ratio, respectively. It is obvious that the σ_y, σ_b, σ_f, δ_e, and δ values of the as-cast or cold-rolled alloys are all increased with the increase of oxygen content. Moreover, the σ_y, σ_b, and σ_f values can be dramatically increased by cold rolling, while the deformation ability decreases sharply. Considering the above experimental result, i.e., the grain size of the 1O or 2O alloys is much coarser than that of the 0O alloy, the strengthening mechanism of these alloys cannot be attributed to grain refinement. According to Saito's model, Zr-O clusters would be generated in the Ti-Ta-Zr-Nb alloys with the addition of oxygen, which will strengthen the alloys by means of inhibiting the movement of dislocations [4]. Within a certain range of oxygen content, the number of Zr-O clusters will increase with increasing oxygen content, leading to the increase in the strength as well as the decrease in the deformation ability of the alloys.

Hardness is an important performance index for metal materials. Fig. 3(b) displays the dependence of the hardness of the as-cast and cold-rolled alloys on oxygen content. Every value shown in Fig. 3(b) is the average value of 20 different positions on the samples. It is obvious that the hardness of the alloys can be improved by the increase of oxygen content for the as-cast and cold-rolled alloys.

3.3. Fracture morphology

As mentioned above, the tensile strength can be improved but the plastic deformability could be deteriorated by cold rolling, which can also be verified by the typical fracture morphology of the tensile samples shown in Fig. 4. It can be seen from Fig. 4(a) that the fracture of the as-cast alloy contains a large amount of deep and equiaxed dimples, demonstrating that the alloy experiences a strong plastic deformation process before fracture. As for the cold-rolled alloys, although there are some dimples in the fracture, the dimples are much shallower and smoother and show some characteristic features like those of amorphous alloy, e.g., vein patterns on the compressive fracture surface at room temperature [18-19], indicating that this alloy is poor in the plastic deformation ability.

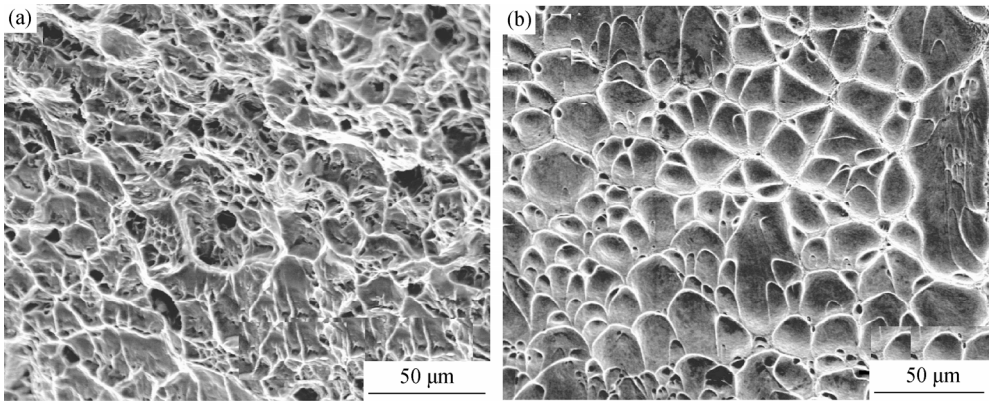

Fig. 4. SEM images of the tensile fracture for as-cast (a) and cold-rolled 1O alloys (b).

3.4. TEM analysis

It is known that the usual morphology of martensite can be presented in the band or needle shape. However, as seen under TEM observations in Fig. 5(a), there exists a kind of V-shape microstructure in the as-cast 0O alloy, consisting of lamellar α″ and β phases alternatively. The microstructure of the 1O or 2O alloy is relatively simple and is only composed of a single β phase. No similar V-shape morphology can be observed in the 1O or 2O alloy under TEM observations, as shown in Figs. 5(b) and 5(c). From this perspective, it can be concluded that the addition of oxygen may inhibit the phase transformation from β to α″, which is in accordance with previous results drawn from XRD patterns in this study. To investigate the influence of cold rolling on microstruc-

tural evolution in the alloy, the TEM image of the cold-rolled 0O alloy is also shown in Fig. 5(d). The alloy after cold rolling remains in the alternative or coexistence of α″ and β phases, but the V-shape morphology characteristic disappears. Comparing Fig. 5(a) to Fig. 5(d), we can find that the width of lamellar α″ phase is different in the as-cast and cold-rolled alloys. The width of white lamellar V-shaped α″ phase in the as-cast alloy is about 30 nm, but the lamellar in the cold-rolled alloy becomes much bigger and its width reaches to about 90 nm. Therefore, combined with the previous XRD analysis, it could be inferred that the volume fraction of α″ phase increases after cold rolling.

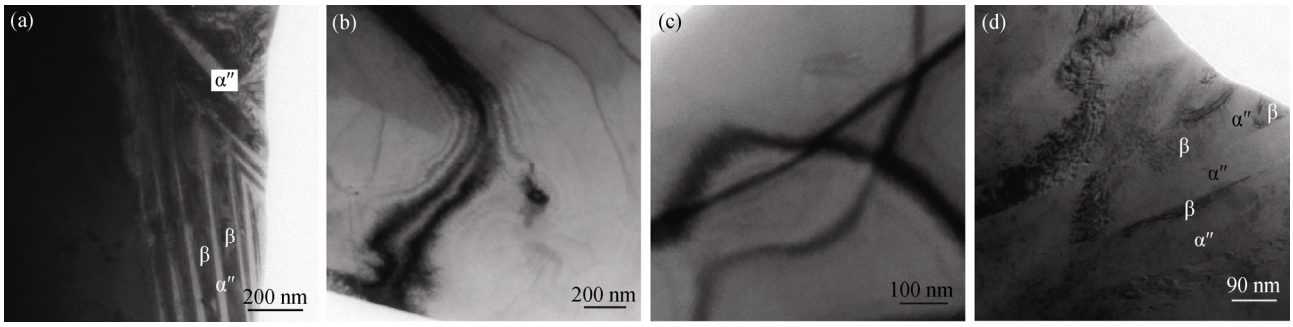

Fig. 5. TEM morphologies of the alloys: (a) as-cast 0O alloy; (b) as-cast 1O alloy; (c) as-cast 2O alloy; (d) cold-rolled 0O alloy.

Fig. 6 shows the high-resolution transmission electron microscopy (HR-TEM) images of the boundary between α″ and β phases. The inset in the upper right corner of Fig. 6 is the selected area diffraction (SAD) pattern along the $[001]_\beta$ direction of the same area. From the HR-TEM image shown in Fig. 6, the interplanar spacing of $(110)_\beta$ can be measured to be about 0.237 nm, which has good agreement with the calculation value from the SAD pattern. Moreover, some planes parallel to the $(110)_\beta$ plane could be found in the α″ phase and its interplanar spacing measured from the HR-TEM image is also about 0.237 nm, indicating that this kind of plane is $(002)_{\alpha''}$.

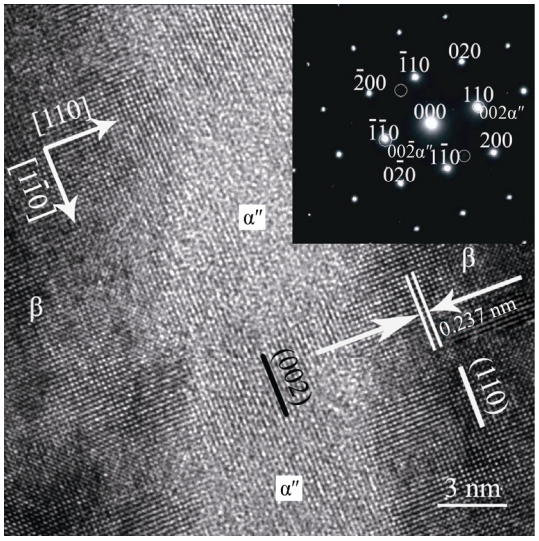

Fig. 6. HR-TEM image of the α″/β phase boundary in the as-cast 0O alloy.

4. Conclusions

(1) Oxygen can stabilize β phase and the phase transformation from β to α″ in the alloy could be inhibited by the addition of oxygen. The single β-Ti alloy could be fabricated easily by adding oxygen element.

(2) Although the grain size of the alloy becomes coarser, the elastic deformation ratio, strength, and hardness could be improved by the addition of oxygen.

(3) The strength of the alloy could be increased by cold rolling but the plastic deformation ability could be decreased dramatically. The fracture model of the alloy transfers from plastic to brittle ones after cold rolling.

References

[1] S. Ankem and C.A. Greene, Recent developments in microstructure/property relationships of beta titanium alloys, *Mater. Sci. Eng. A*, 263(1999), p.127.

[2] T. Kasuga, M. Nogami, M. Niinomi, and T. Hattori, Bioactive calcium phosphate invert glass-ceramic coating on β-type Ti-29Nb-13Ta-4.6Zr alloy, *Biomaterials*, 24(2003), p.283.

[3] M. Abdel-Hady, K. Hinoshita, and M. Morinaga, General approach to phase stability and elastic properties of β-type Ti-alloys using electronic parameters, *Scripta Mater.*, 55(2006), p.477.

[4] T. Saito, T. Furuta, J.H. Hwang, S. Kuramoto, K. Nishino, N. Suzuki, R. Chen, A. Yamada, K. Ito, Y. Seno, T. Nonaka, H. Ikehata, N. Nagasako, C. Iwamoto, Y. Ikuhara, and T. Sakuma, Multifunctional alloys obtained via dislocation-free plastic deformation mechanism, *Science*, 300(2003), p.464.

[5] T. Furuta, S. Kuramoto, J.H. Hwang, K. Nishino, and T. Saito, Elastic deformation behavior of multi-functional Ti-Nb-Ta-

Zr-O alloys, *Mater. Trans.*, 46(2005), p.3001.

[6] S. Kuramoto, T. Furuta, J.H. Hwang, K. Nishino, and T. Saito, Elastic properties of Gum Metal, *Mater. Sci. Eng. A*, 442(2006), p.454.

[7] M.Y. Gutkin, T. Ishizaki, S. Kuramoto, and I.A. Ovid'ko, Nanodisturbances in deformed Gum Metal, *Acta Mater.*, 54(2006), p.2489.

[8] S. Kuramoto, T. Furuta, J.H. Hwang, K. Nishino, and T. Saito, Plastic deformation in a multifunctional Ti-Nb-Ta-Zr-O Alloy, *Metall. Mater. Trans. A*, 37(2006), p.657.

[9] M.Y. Gutkin, T. Ishizaki, S. Kuramoto, I.A. Ovid'ko, and N.V. Skiba, Giant fault in deformed Gum Metal, *Int. J. Plast.*, 24(2008), p.1333.

[10] E. Withey, M. Jin, A. Minor, S. Kuramoto, D.C. Chrzan, and J.W. Morrism Jr, The deformation of "Gum Metal" in nanoindentation, *Mater. Sci. Eng. A*, 493(2008), p.26.

[11] T. Yano, Y. Murakami, D. Shindo, and S. Kuramoto, Study of the nanostructure of Gum Metal using energy-filtered transmission electron microscopy, *Acta Mater.*, 57(2009), p.628.

[12] J.W. Morris Jr, Y. Hanlumyuang, M. Sherburne, E. Withey, D.C. Chrzan, S. Kuramoto, Y. Hayashi, and M. Hara, Anomalous transformation-induced deformation in <110> textured Gum Metal, *Acta Mater.*, 58(2010), p.3271.

[13] S. Kuramoto, T. Furuta, J.H. Hwang, *et al.*, Ti-2003 science and technology, [in] *Proceedings of 10th World Conference on Titanium*, Hamburg, 2004, p.1527.

[14] Q.Q Wei, L.Q. Wang, Y.F. Fu, J.N. Qin, W.J. Lu, and D. Zhang, Influence of oxygen content on microstructure and mechanical properties of Ti-Nb-Ta-Zr alloy, *Mater. Des.*, 32(2011), p.2934.

[15] F.Q. Hou, S.J. Li, Y.L. Hao, and R. Yang, Nonlinear elastic deformation behaviour of Ti-30Nb-12Zr alloys, *Scripta Mater.*, 63(2010), p.54.

[16] J.I. Qazi, B. Marquardt, L.F. Allard, and H.J. Rack, Phase transformations in Ti-35Nb-7Zr-5Ta-(0.06-0.68)O alloys, *Mater. Sci. Eng. C*, 25(2005), p.389.

[17] M. Tahara, H.Y. Kim, T. Inamura, H. Hosoda, and S. Miyazaki, Lattice modulation and superelasticity in oxygen-added β-Ti alloys, *Acta Mater.*, 59(2011), p.6208.

[18] Q.S. Zhang, H.F. Zhang, B.Z. Ding, and Z.Q. Hu, Compressive fracture of $Zr_{55}Al_{10}Ni_5Cu_{30}$ bulk amorphous alloy at high temperature, *Mater. Sci. Eng. A*, 360(2003), p.280.

[19] Z.Q. Liu, R. Li, H. Wang, and T. Zhang, Nitrogen-doping effect on glass formation and primary phase selection in Cu-Zr-Al alloys, *J. Alloys Compd.*, 509(2011), p.5033.